Towards Efficient Control of Mobile Network-Enabled UAVs

Hamed Hellaoui[1], Ali Chelli[2], Miloud Bagaa[1], Tarik Taleb[1,3], and Matthias Pätzold[2]

[1]Communications and Networking Department, Aalto University, Finland. Email:firstname.lastname@aalto.fi
[2]University of Agder, 4898 Grimstad, Norway. Emails:{ali.chelli, matthias.paetzold}@uia.no
[3]University of Oulu, 90570 Oulu, Finland.

Abstract— **The efficient control of mobile network-enabled unmanned aerial vehicles (UAVs) is targeted in this paper. In particular, a *downlink scenario* is considered, in which control messages are sent to UAVs via cellular base stations (BSs). Unlike terrestrial user equipment (UEs), UAVs perceive a large number of BSs, which can lead to increased interference causing poor or even unacceptable throughput. This paper proposes a framework for efficient control of UAVs. First, a communication model is introduced for flying UAVs taking into account interference, path loss and fast fading. The characteristics of UAVs make such model different compared to traditional ones. Thereafter, in order to ensure the efficient control, a solution is proposed for reducing interference. This is achieved by efficiently assigning sub-carriers to the UAVs in a way to reduce interference. A maximum independent set formulation is proposed along with an algorithm for optimal sub-carrier allocation. The obtained results demonstrate the efficiency of the proposed solution in terms of enhancing the link quality of UAVs.**

I. INTRODUCTION

Unmanned aerial vehicles (UAVs), also known as drones, have tremendous applications in various areas [1]. In order to boost their benefits, a huge interest was recently manifested from both scientific and industrial communities to use mobile networks as a communication infrastructure for UAVs. This would mainly provide two benefits. First, it will be possible to control the drones beyond the line of sight. This would push the coverage range of the UAVs and allow them to provide new services and applications. Moreover, mobile networks are uniquely positioned to improve the safety of UAV operations. The advances achieved by cellular networks (LTE, 5G and beyond), can provide higher data rates, reduced latency, and higher throughput for UAV applications. All these features make mobile networks the key to unlocking the potential of drones.

In order to enable mobile network-based UAVs, several issues need to be addressed. In this context, interference is considered as a limiting factor challenging the development of this technology. Indeed, the number of base stations (BSs) perceived by a drone increases as the drone's height increases. Real field experiments showed that a flying UAV can detect more than 10 cells. This is mainly due to the almost free-space propagation conditions between the UAVs and the terrestrial BSs. Consequently, when it comes to the downlink scenario at high levels of altitude, a UAV witnesses high interference levels from non-serving BSs. Real field tests performed by the 3rd Generation Partnership Project

(3GPP) have revealed that flying UAVs may experience very poor downlink throughput compared to terrestrial user equipment (UEs) [2]. Thereby, the communication with the UAVs could be impaired or even lost. Given the critical nature of UAVs, a small latency cannot be tolerated, not to mention losing the communication. These facts highlight the control issue in mobile network-enabled UAVs and enforce the requirements for efficient solutions [3].

In the literature, some works have studied the use of edge computing for UAVs (e.g., [4]–[6]). However, the communication link quality is not the focus of those works. In addition, the UAVs' interference issue was tackled in the literature with methods such as power optimization and path adjusting (e.g., [7], [8]). Sub-carrier assignment is a promising technique that can mitigate the interference impact and has not yet been considered for cellular network-connected UAVs. This underpins the focus of this article wherein a framework for efficient control of mobile network-enabled UAVs is proposed. The major contributions of this work are the following:

- We propose a realistic system model for mobile network-enabled UAVs (Section II). This system model accounts for most of the propagation phenomena experienced by wireless signals, such as path loss, fast fading, and interference. Analytical expressions are derived for the outage probability of UAVs on the downlink.
- Unlike existing works for handling the issue of interference in cellular network-connected UAVs, a solution is proposed based on sub-carrier assignment (Section III). We formulate the sub-carrier assignment problem using graph theory, as a maximum independent sets problem, and we propose an algorithm for sub-carrier assignment.
- The paper also provides numerical results of the quality of communication and demonstrates the crucial role of sub-carrier assignment techniques (Section IV). It reveals that the proposed sub-carrier assignment technique can ensure an improvement of the link quality compared to the case of random sub-carrier allocation.

II. SYSTEM MODEL

We consider a network of BSs providing connectivity on the downlink for flying UAVs and UEs on the ground. Beside investigating the QoE of UAVs in our work, we also study the UEs' QoE for the sake of comparison. Let $\mathbb{B}$, $\mathbb{V}$, and $\mathbb{U}$ denote the set of BSs, UAVs, and UEs, respectively.

The BSs employ an orthogonal frequency division multiple access (OFDMA) technique to serve their devices. Due to the orthogonality among the sub-carriers per cell, intra-cell interference is negligible. However, as shown in Fig. 1, interference can be caused by non-serving BSs.
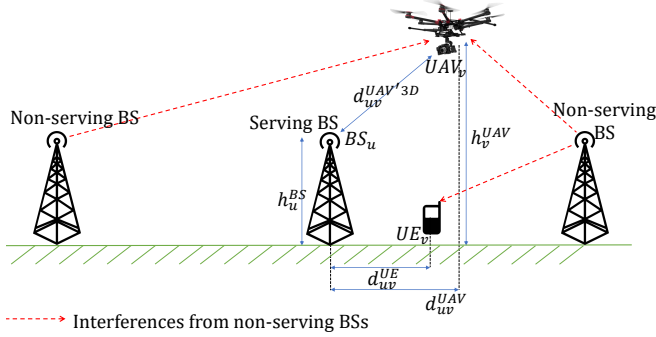

Fig. 1: System model.

Let u denote the serving BS and v the receiving device. The complex channel gain between these two nodes is referred to as α_{uv}. The non-serving BS t causes interference to the receiving device v. We assume that the cardinality of $\mathbb{B}$ is equal to $N+1$ which implies that the number of non-serving/interfering BSs is equal to N. The complex channel gain between the non-serving BS t and the device v is denoted by α_{tv}. The received signal y_v at the device v is the sum of the desired signal from the serving BS, the interference from N non-serving BSs, and the noise, i.e.,

$$y_v = \alpha_{uv}\sqrt{P_u}x_u + \sum_{t=1}^{N}\alpha_{tv}\sqrt{P_t}x_t + n_v \qquad (1)$$

where x_u and x_t refer to the transmitted symbols by the BSs u and t, respectively. The transmission powers employed by the BSs u and t are denoted by P_u and P_t, respectively. The noise n_v is modelled by a zero-mean complex additive white Gaussian noise process with variance N_0. The instantaneous received signal-to-noise ratio (SNR) for the link uv, γ_{uv}, can be expressed as

$$\gamma_{uv} = P_u/N_0|\alpha_{uv}|^2. \qquad (2)$$

If the receiving device v is a UAV, the underlying fading characteristics are substantially different compared to the case where the receiving device is a UE. For the UE, we use the path loss expression provided by 3GPP [9]

$$PL_{uv}^{UE} = 15.3 + 37.6\log_{10}\left(d_{uv}^{UE}\right) \qquad (3)$$

where d_{uv}^{UE} refers to the distance in meter between the BS u and the UE v as shown in Fig. 1. The path loss equation in (3) is valid for a carrier frequency of 2 GHz. We assume a Rayleigh distribution for the fast fading associated with the UEs. The mean SNR of the link between the UE device v and the BS u is denoted by $\bar{\gamma}_{uv}$ and can be expressed as

$$\bar{\gamma}_{uv} = P_u^{UE}/N_0 \times 10^{-\frac{PL_{uv}^{UE}}{10}}. \qquad (4)$$

The instantaneous received signal-to-interference-plus-noise ratio (SINR) for the link uv can be defined as

$$SINR_{uv} = \gamma_{uv}/(1 + \sum_{t=1}^{N}\gamma_{tv}). \qquad (5)$$

Theorem 1: A BS u serving a UE v fails in transmitting its packets on the downlink iff the $SINR_{uv}$ falls below a threshold γ_{th}. This event, called outage, occurs with a probability $P_{out,uv}^{UE}$ that can be expressed as

$$P_{out,uv}^{UE}(\gamma_{th}) = 1 + \exp\left(-\frac{\gamma_{th}}{\bar{\gamma}_{uv}}\right)\sum_{t=1}^{N}\frac{\alpha_t}{\frac{\gamma_{th}}{\bar{\gamma}_{uv}} + \frac{1}{\bar{\gamma}_{tv}}} \qquad (6)$$

where α_t are unique values satisfying the following equality (fractional decomposition)

$$\prod_{t=1}^{N}(1 - x\bar{\gamma}_{tv})^{-1} = \sum_{t=1}^{N}\frac{\alpha_t}{x - \frac{1}{\bar{\gamma}_{tv}}}. \qquad (7)$$

Proof: See Appendix I. ∎

For the case where the receiving device is a UAV, the path loss differs depending on the line-of-sight (LoS) and the non-line-of-sight (NLoS) conditions. The LoS communication results in a better QoE compared to the NLoS one. We consider in our proposed solution the path loss equation provided by 3GPP as [2]

$$PL_{uv}^{UAV} = \begin{cases} 28.0 + 22\log_{10}(d_{uv}^{UAV'3D}) + 20\log_{10}(f_c) \\ \qquad \text{for LoS link} \\ \\ -17.5 + (46 - 7\log_{10}(h_v^{UAV}))\log_{10}(d_{uv}^{UAV'3D}) \\ +20\log_{10}(\frac{40\pi f_c}{3}) \qquad \text{for NLoS link} \end{cases} \qquad (8)$$

where h_v^{UAV} is the altitude of the UAV v and $d_{uv}^{UAV'3D}$ is the Euclidean distance between the BS u and the UAV v as shown in Fig. 1. The carrier frequency is denoted by f_c and is set to 2 GHz. The probability of a LoS condition P_{uv}^{LoS} is determined as [2]

$$P_{uv}^{LoS} = \begin{cases} 1 & \text{if } h_v^{UAV} > 100 \\ 1 & \text{if } d_{uv}^{UAV} \leq d_1 \\ \frac{d_1}{d_{uv}^{UAV}} + \exp\left(\frac{-d_{uv}^{UAV}}{p_1}\right)\left(1 - \frac{d_1}{d_{uv}^{UAV}}\right) & \text{if } d_{uv}^{UAV} > d_1 \end{cases} \qquad (9)$$

where $p_1 = 4300\log_{10}(h_v^{UAV}) - 3800$ and $d_1 = \max(460\log_{10}(h_v^{UAV}) - 700, 18)$. The symbol d_{uv}^{UAV} refers to the 2D distance between the UAV v and the serving BS u as illustrated in Fig. 1. It is worth noting that the NLoS probability, P_{uv}^{NLoS}, can be obtained as $P_{uv}^{NLoS} = 1 - P_{uv}^{LoS}$. The corresponding fast fading follows a Nakagami-m distribution for LoS links, and a Rayleigh distribution for NLoS links. The mean SNRs of the LoS and NLoS links are denoted by A_{uv} and B_{uv}, respectively, and are obtained as

$$\begin{cases} A_{uv} & = P_{uv}^{LoS} \times P_u/N_0 \times 10^{-\frac{PL_{uv}^{UAV}}{10}} \\ B_{uv} & = P_{uv}^{NLoS} \times P_u/N_0 \times 10^{-\frac{PL_{uv}^{UAV}}{10}}. \end{cases} \qquad (10)$$

Theorem 2: The downlink outage probability for a BS u serving a UAV v is expressed as

$$P_{out,uv}^{UAV}(\gamma_{th}) = \sum_{j=1}^{m}\left(\beta_{1j}\frac{(-1)^j}{(j-1)!}\left(\frac{m}{A_{uv}}\right)^{-j}\left(\Gamma(j) + \sum_{t=1}^{N}\alpha'_t f_{j,1}(B_{tv})\right.\right.$$
$$\left.\left. - \sum_{t=1}^{N}\sum_{j'=1}^{m}\frac{\alpha_{t,j'}(-1)^{j'}}{(j'-1)!}f_{j,j'}(A_{tv}/m)\right)\right) - \beta_{21}B_{uv}\left(1 + \exp(-\frac{\gamma_{th}}{B_{uv}})\right.$$
$$\left.\left(\sum_{t=1}^{N}\frac{\alpha'_t}{\frac{\gamma_{th}}{B_{uv}} + \frac{1}{B_{tv}}} - \sum_{t=1}^{N}\sum_{j=1}^{m}\frac{\alpha_{t,j}}{\left(\frac{\gamma_{th}}{B_{uv}} + \frac{m}{A_{tv}}\right)^j}\frac{(-1)^j}{(j-1)!}\Gamma(j)\right)\right) \qquad (11)$$

where β_{1j}, β_{21}, α'_t and $\alpha_{t,j}$ are unique values satisfying the two following equations (fractional decomposition)

$$\left(1-x\frac{A_{uv}}{m}\right)^{-m}(1-xB_{uv})^{-1} = \sum_{j=1}^{m}\frac{\beta_{1j}}{(x-\frac{m}{A_{uv}})^{j}} + \frac{\beta_{21}}{(x-\frac{1}{B_{uv}})} \qquad (12)$$

$$\prod_{t=1}^{N}(1-xB_{tv})^{-1}(1-\frac{xA_{tv}}{m})^{-m} = \sum_{t=1}^{N}\frac{\alpha_{t}'}{x-\frac{1}{B_{tv}}} + \sum_{t=1}^{N}\sum_{j=1}^{m}\frac{\alpha_{t,j}}{\left(x-\frac{m}{A_{tv}}\right)^{j}}. \qquad (13)$$

The function $f_{j,j'}(S)$ is provided as

$$f_{j,j'}(S) = \sum_{p=1}^{n} S^{j'}(\theta_p)^{j'-1}\lambda_p\Gamma\left(j,\frac{m\gamma_{th}(\theta_p S+1)}{A_{uv}}\right) \qquad (14)$$

where λ_p and θ_p denote the weight and the zero factors of the n-th order Laguerre polynomials, respectively [10]. $\Gamma(a,z)$ is the upper incomplete gamma function defined as $\Gamma(a,z) = \int_z^\infty t^{a-1}e^{-t}dt$.

Proof: See Appendix I. ∎

Theorems 1 and 2 provide the outage probability of the downlink for a UE and a UAV, respectively. These expressions have been derived taking into account path loss, fast fading, and interference. This makes our proposed system model realistic since it reflects most of the propagation phenomena that the wireless signal undergoes. To the best of the authors' knowledge, the expressions of the outage probabilities provided in Theorems 1 and 2 are novel results.

III. CHANNEL ASSIGNMENT FOR UAVS CONTROL

Given their critical nature, efficient control of UAVs is of utmost importance. Therefore, it is necessary to improve the quality of the communication on the downlink by reducing the outage probability of UAVs. By carefully investigating the behavior of the outage probability of UAVs provided in Theorem 2, we notice that the outage probability increases as the value of the parameters A_{tv} and B_{tv} increases. This implies that if we reduce the interference created by non-serving BSs, we can improve the link quality for UAVs. As the flying UAVs can perceive a large number of BSs, they suffer from higher level of interference compared to UEs.

To enhance the control of UAVs, we propose a solution to reduce the level of interference at the UAVs. This is achieved by efficiently assigning sub-carriers to the UAVs, such that the overall interference in the network is reduced. To this end, we use graph theory to formulate the problem of sub-carrier assignment as a maximum independent set problem [11]. Using the heuristic algorithm proposed in [12], we obtain an optimal solution for the sub-carrier assignment such that the average outage probability per link is minimized. Let's consider the undirected graph $\mathbb{G} = (\mathbb{V},\mathbb{E})$, where the nodes represent the set of UAVs. The vertices of the graph are the UAVs. Let v_1 and v_2 be two UAVs being served by the BSs u_1 and u_2, respectively. We denote by $I_{u_1v_2}$ the interference created by the BS u_1 at the UAV v_2 and $I_{u_2v_1}$ the interference created by the BS u_2 at the UAV v_1. If $I_{u_1v_2}$ or $I_{u_2v_1}$ exceeds a threshold value I_{th}, then the vertices v_1 and v_2 are connected by an edge e in the graph $\mathbb{G}$, which can be expressed by the following equation

$$\text{if }\begin{cases}I_{u_1v_2} > I_{th}\\ OR\\ I_{u_2v_1} > I_{th}\end{cases} \Longrightarrow e = (v_1,v_2) \in \mathbb{E} \qquad (15)$$

Two vertices v_1 and v_2 are connected by an edge e, if their serving BSs u_1 and u_2 use the same sub-carrier to communicate with them, the level of interference $I_{u_1v_2}$ or $I_{u_2v_1}$ exceeds the threshold I_{th}. Subsequently, the quality of communication for the UAVs v_1 and v_2 will be poor. On the other hand, for two vertices that are not connected in the graph $\mathbb{G}$, even if their serving BSs assign to each vertex (i.e., UAV) the same sub-carrier, the level of interference is below the threshold I_{th} and we can insure a good link quality. Following this line of thoughts, we need to determine the sets comprising nodes that are not connected by edges, such sets are independent. Then we assign to all the terms of the same set the same sub-carrier. In this way, the interference is reduced in the network. Therefore, to obtain the best sub-carrier allocation, we need to determine the maximum independent sets in the graph $\mathbb{G}$. Afterwards, we assign the same sub-carrier to all the nodes belonging to the same maximum independent set.

Definition 1: *An independent set is a subset of UAVs $\mathbb{V}_c \subseteq \mathbb{V}$ using the same sub-carrier, and no two nodes in $\mathbb{V}_c$ are adjacent. A set is called maximum if it has the maximum cardinality.*

In Fig. 2, we visually illustrate the different steps of our sub-carrier assignment algorithm. The dashed red lines indicate the interference created by BSs 1 and 2 in each UAV. If we do not use a threshold on the interference level, we end up with a complete graph, where each node is connected to all the remaining nodes in the network. In such a situation, there exists no independent set. By using the rule in (15), we can tolerate interference that is below the predefined threshold I_{th}. Fig. 2(b) illustrates this principle by showing the links for which the interference exceeds the threshold I_{th}. The graph associated with the scenario in Fig. 2(b) is provided in Fig. 2(c). One can notice that in this graph some nodes have no edge connecting them directly and are consequently independent. Hence, their corresponding BSs can assign to them the same sub-carrier without breaking the rule in (15). An illustration of maximum independent sets construction is provided in Fig. 2(d), where nodes with the same color belong to the same set.
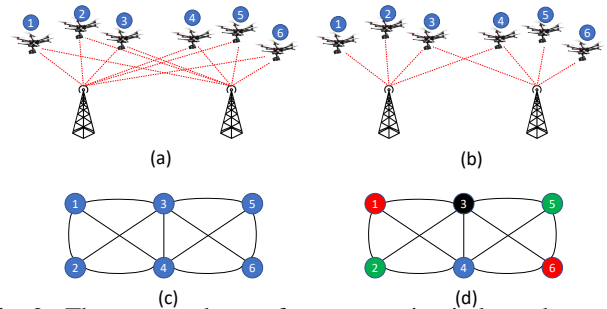

Fig. 2: The proposed steps for constructing independent sets.

Algorithm 1 shows the proposed channel assignment procedure. The set of edges are constructed (line 2 of Algorithm 1) based on (15). We determine a maximum independent set from the graph $\mathbb{G}$ (line 5 of Algorithm 1) using the heuristic algorithm proposed in [12] and store them in g. The BSs

serving the nodes in set g can use the same sub-carrier to communicate with these nodes. The function *assign_ch(g)* (line 6 of Algorithm 1) assigns the same sub-carrier to the nodes in g. The nodes in g are then removed from the set of vertices (line 7) and the graph $\mathbb{G}$ is reconstructed without the set g (line 8). The same procedure is repeated on the newly generated graph $\mathbb{G}$. This allows establishing other independent sets and assigning to each one a sub-carrier.

Algorithm 1 Channel assignment algorithm.

1: **procedure** CHANNEL ASSIGNMENT OPTIMIZATION
    Input: $\mathbb{V}$, $\mathbb{B}$, I_{th}
2:     $\mathbb{E}$ = construct_edges($\mathbb{V}$, $\mathbb{B}$, I_{th})
3:     $\mathbb{G} = (\mathbb{V}' = \mathbb{V}, \mathbb{E})$
4:     **repeat**
5:         g = get_max_ind_set($\mathbb{G}$)
6:         assign_ch(g)
7:         $\mathbb{V}' = \mathbb{V}' \setminus g$
8:         $\mathbb{G} = (\mathbb{V}', \mathbb{E})$
9:     **until** $\mathbb{V}' = \emptyset$

IV. PERFORMANCE EVALUATION

The proposed communication model is implemented considering a Nakagami model with parameter $m = 2$, a carrier frequency f_c equal to 2 GHz, and a noise variance N_0 of -130 *dBm* [13]. The evaluation is performed in a 1 km x 1 km square area with 12 BSs and different devices being randomly deployed. The maximum transmission power of each BS is 40 W. The altitude of the UAVs is randomly chosen between 22.5 m and 300 m (the path loss expression provided in [2] is valid within this range of altitude). The function *assign_ch(g)* assigns to the corresponding UAVs the sub-carrier with less transmission power.

The sensitivity threshold γ_{th} indicates the level that the SINR should exceed so that the packet is received successfully, and its value has a significant impact on the QoE study. Fig. 3(a) illustrates the obtained average outage probability for different values of the threshold γ_{th}. As we can see, the outage probability decreases as the sensitivity threshold γ_{th} decreases. It reflects indeed the ability of a receiver device to detect weak signals and its value needs to be adequately chosen. In addition, Fig. 3(a) shows that the UAVs experience higher outage probability compared to UEs. These results confirm the real field experiments performed by 3GPP which revealed that UAVs experience worse QoE compared to terrestrial UEs for the downlink scenario. This is mainly due to close to free-space propagation conditions that characterize the BS-UAV channel. This implies that a UAV receives interference signals from many neighboring BSs. This underpins the need for efficient control of the UAVs so that the outage probability of the BS-UAV link is maintained below a certain level. It is worth noting that both curves in Fig. 3(a) have been obtained by considering 50 UEs and 50 UAVs in our simulation.

In addition, we have evaluated the proposed channel assignment solution. We considered a scenario of sequentially adding UAVs to the area, wherein 50 UEs are already deployed and connected. The obtained results are shown in Fig. 3(b). We can see that the proposed solution efficiently enhance the quality of communication UAVs would experience starting from few numbers of UAVs. In this figure, we consider two sub-carrier assignment methods: (i) random assignment and (ii) assignment based on the Algorithm 1 proposed in Section IV. Indeed, as there are already deployed devices, adding UAVs to the network and assigning sub-carriers to them randomly without using an optimal strategy leads to high outage probability for the UAVs. Note as well that the outage probability increases significantly with the number of added UAVs if a random assignment is used. Compared to the random assignment approach, our proposed assignment solution allows to maintain the outage probability very low even if a large number of UAVs is added to the network. For instance, if 50 UAVs are added to the network, the outage probability is reduced from 35% to 5% by using our proposed sub-carrier assignment strategy. These results come to confirm the importance of optimizing sub-carrier assignment for flying UAVs and demonstrate the efficiency of the proposed solution.

Fig. 4 provides a 3D visualization of the network topology. Here, we consider two outage probability thresholds: 0.1 and 0.2. Red triangles denote UAVs with an outage probability larger than 0.2, green ones for UAVs with an outage probability less than 0.1, while blue ones refer to those with an outage probability between the two threshold. Fig. 4 illustrates the impact of UAV position on the QoE and highlights the importance of sub-carrier allocation in improving the link quality for UAV. Note that Algorithm 1 has been used in Figs. 4(a) and (b). The results in Fig. 4(a) have been obtained by using 25 UAVs, while for Fig. 4(b), we used 50 UAVs. Out of 50 UAVs, 10 UAVs (20%) have an outage probability between the two thresholds in Fig. 4(b), whereas only 3 UAVs (6%) have poor link quality (larger than 0.2). Almost all the UAVs in Fig. 4(a) have good link quality. These facts capture the importance of the proposed sub-carrier assignment solution in enhancing the communication quality at different altitude. This is required in many applications where UAVs must react in real-time to the received control messages.

V. CONCLUSION

This paper addressed the efficient control of mobile network-enabled UAVs. It introduced a realistic system model for UAVs that accounts for path loss, interference, and fast fading. We derived novel analytical expressions for the outage probability of UAVs. In this context, we investigated the problem of optimal sub-carrier assignment and formulated it using graph theory. The paper proposed a novel scheme for sub-carrier assignment that allows reducing the interference levels significantly at the UAVs, which yield a reduced outage probability and an enhanced QoE. Our analysis illustrated the usefulness of the proposed scheme in maintaining acceptable outage even if a large number of UAVs is added to the network.
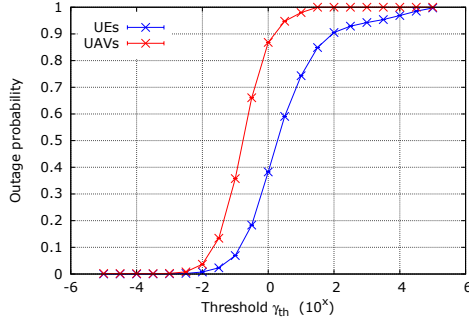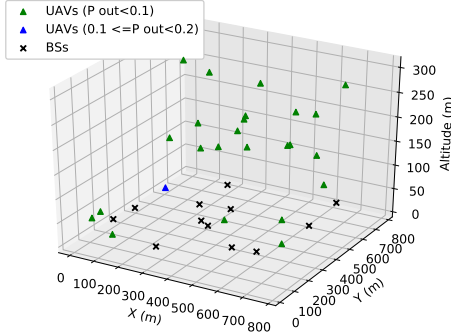
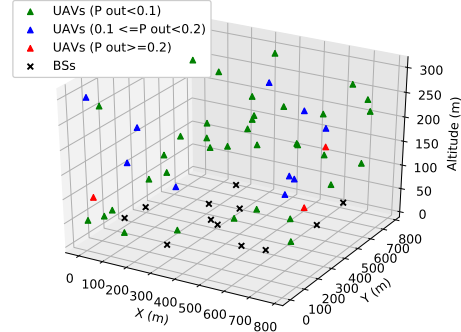(a) Outage probabilities $P_{out,uv}(\gamma_{th})$ for different threshold values γ_{th}.
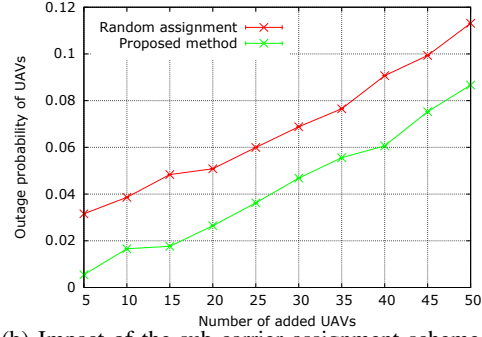
(b) Impact of the sub-carrier assignment scheme on the outage probability of UAVs.

Fig. 3: Evaluations of the outage probability.

(a) 25 UAVs.

(b) 50 UAVs.

Fig. 4: Experienced quality of communication of deployed UAVs.

REFERENCES

[1] N. H. Motlagh, T. Taleb, and O. Arouk, "Low-altitude unmanned aerial vehicles-based Internet of Things services: Comprehensive survey and future perspectives," *IEEE Internet of Things Journal*, vol. 3, no. 6, pp. 899–922, Dec. 2016.

[2] 3GPP, "Study on enhanced LTE support for aerial vehicles," *Technical Report, 3GPP TR 36.777*, 2017. [Online]. Available: http://www.3gpp.org/ftp//Specs/archive/36_series/36.777/

[3] H. Hellaoui, O. Bekkouche, M. Bagaa, and T. Taleb, "Aerial control system for spectrum efficiency in uav-to-cellular communications," *IEEE Communications Magazine*, vol. 56, no. 10, pp. 108–113, OCTOBER 2018.

[4] O. Bekkouche, T. Taleb, and M. Bagaa, "UAVs Traffic Control based on Multi-Access Edge Computing," in *2018 IEEE Global Communications Conference (GLOBECOM 2018)*, Dec. 2018.

[5] S. Ouahouah, T. Taleb, J. Song, and C. Benzaid, "Efficient offloading mechanism for UAVs-based value added services," in *2017 IEEE International Conference on Communications (ICC)*, May 2017, pp. 1–6.

[6] N. H. Motlagh, M. Bagaa, and T. Taleb, "Uav-based iot platform: A crowd surveillance use case," *IEEE Communications Magazine*, vol. 55, no. 2, pp. 128–134, February 2017.

[7] U. Challita, W. Saad, and C. Bettstetter, "Deep reinforcement learning for interference-aware path planning of cellularconnected uavs," in *International Conference on Communications (ICC)*, 2018.

[8] H. Hellaoui, A. Chelli, M. Bagaa, and T. Taleb, "Towards Mitigating the Impact of UAVs on Cellular Communications," in *2018 IEEE Global Communications Conference (GLOBECOM 2018)*, Dec. 2018.

[9] 3GPP, "Radio frequency (RF) system scenarios," *Technical Report, (TSG) RAN WG4*, 2000. [Online]. Available: http://www.3gpp.org/ftp//Specs/archive/25_series/25.942/

[10] M. Abramowitz and I. A. Stegun, *Handbook of Mathematical Functions: With Formulas, Graphs, and Mathematical Tables*. Courier Corporation, 1964.

[11] R. J. Trudeau, *Introduction to Graph Theory*. New York: Dover Publications, 1993.

[12] R. Boppana and M. M. Halldórsson, "Approximating maximum independent sets by excluding subgraphs," *BIT Numerical Mathematics*, vol. 32, no. 2, pp. 180–196, Jun 1992. [Online]. Available: https://doi.org/10.1007/BF01994876

[13] A. F. Molisch, *Wireless Communications*. Chichester: John Wiley & Sons, 2005.

[14] X. Cui, Q. Zhang, and Z. Feng, "Outage performance for maximal ratio combiner in the presence of unequal-power co-channel interferers," *IEEE Communications Letters*, vol. 8, no. 5, pp. 289–291, May 2004.

[15] A. Papoulis and S. U. Pillai, *Probability, Random Variables, and Stochastic Processes*, 4th ed. McGraw-Hill, 2002.

APPENDIX I
APPENDIX: PROOF OF THEOREMS 1 AND 2

To derive the outage probability expressions, we recall that the expression of the SINR is given by

$$SINR_{uv} = \frac{\gamma_{uv}}{1 + \sum\limits_{t=1}^{N} \gamma_{tv}} = \frac{\gamma_{uv}}{1 + I} = \frac{\gamma_{uv}}{I'}. \qquad (I.1)$$

By definition, the outage probability for the link uv is given by

$$P_{out}(\gamma_{th}) = P(SINR \leq \gamma_{th}) = P\left(\frac{\gamma_{uv}}{I'} \leq \gamma_{th}\right)$$

$$= E_{I'}\left[P(\gamma_{uv} \leq \gamma_{th}y | I' = y)\right] = \int_{1}^{\infty} F_{\gamma_{uv}}(\gamma_{th}y)P_{I'}(y)dy \qquad (I.2)$$

where $F_{\gamma_{uv}}(x)$ is the cumulative distribution function (CDF) of γ_{uv}, which is computed as $F_{\gamma_{uv}}(x) = \int_0^x P_{\gamma_{uv}}(y)dy$. The term $P_{I'}(y)$ is the probability density function (PDF) of I'. The expressions of these two latter quantities depend on whether the receiver device v is a UE or a UAV.

Case where v is a UE: In this case, $\bar{\gamma}_{uv}$ is provided in (4). The moment generating function (MGF) and the PDF of γ_{uv} can be obtained as

$$M_{\gamma_{uv}}^{UE}(s) = (1 - s\bar{\gamma}_{uv})^{-1} \tag{I.3}$$

$$P_{\gamma_{uv}}^{UE}(x) = \frac{1}{\bar{\gamma}_{uv}} \exp\left(-\frac{x}{\bar{\gamma}_{uv}}\right). \tag{I.4}$$

Then, the MGF of I, which includes all the interfering BSs, can be deduced as

$$M_I(s) = \prod_{t=1}^{N} M_{\gamma_{tv}}(s) = \prod_{t=1}^{N}(1 - s\bar{\gamma}_{tv})^{-1} = \sum_{t=1}^{N} \frac{\alpha_t}{s - \frac{1}{\bar{\gamma}_{tv}}} \tag{I.5}$$

where α_t is obtained using fractional decomposition (multinomial theorem [14]). Note that α_t is the same as in Theorem 1 satisfying (7). By computing the inverse Laplace transform of $M_I(s)$ in (I.5), the PDF $P_I(x)$ of I can be obtained as

$$P_I(x) = \mathcal{L}^{-1}[M_I(s)] = \mathcal{L}^{-1}\left[\sum_{t=1}^{N} \frac{\alpha_t}{s - \frac{1}{\bar{\gamma}_{tv}}}\right] = \sum_{t=1}^{N} \alpha_t(-1)\exp\left(-\frac{x}{\bar{\gamma}_{tv}}\right). \tag{I.6}$$

The PDF $P_{I'}(y)$ of I' is computed by using (I.6) and the fundamental theorem of transformation of random variables [15]. Thus,

$$P_{I'}(y) = \sum_{t=1}^{N} \alpha_t(-1)\exp\left(-\frac{y-1}{\bar{\gamma}_{tv}}\right). \tag{I.7}$$

On the other hand, the CDF $F_{\gamma_{uv}}^{UE}(x)$ of γ_{uv} is determined from (I.4) as

$$F_{\gamma_{uv}}^{UE}(x) = \int_0^x P_{\gamma_{uv}}^{UE}(y)dy = 1 - \exp\left(-\frac{x}{\bar{\gamma}_{uv}}\right). \tag{I.8}$$

Finally, the outage probability is obtained as

$$P_{out}^{UE}(\gamma_{th}) = \int_1^\infty F_{\gamma_{uv}}(\gamma_{th}y)P_{I'}(y)dy = 1 - \int_1^\infty \exp\left(-\frac{\gamma_{th}y}{\bar{\gamma}_{uv}}\right)P_{I'}(y)dy$$

$$= 1 + \exp\left(-\frac{\gamma_{th}}{\bar{\gamma}_{uv}}\right)\sum_{t=1}^{N} \frac{\alpha_t}{\frac{\gamma_{th}}{\bar{\gamma}_{uv}} + \frac{1}{\bar{\gamma}_{tv}}}. \tag{I.9}$$

The result in (I.9) is the same as the outage probability provided in Theorem 1. $\blacksquare$

Case where v is a UAV: In this case, both LoS and NLoS conditions are considered. The terms A_{uv} and B_{uv} are defined in (10) to reflect the mean SNR related to the two conditions. The MGF $M_{\gamma_{uv}}^{UAV}(s)$ of γ_{uv} reads as

$$M_{\gamma_{uv}}^{UAV}(s) = M_{\gamma_{LoS,uv}} M_{\gamma_{NLoS,uv}} = \left(1 - \frac{sA_{uv}}{m}\right)^{-m}(1 - sB_{uv})^{-1}$$

$$= \sum_{j=1}^{m} \frac{\beta_{1j}}{(s - \frac{m}{A_{uv}})^j} + \frac{\beta_{21}}{(s - \frac{1}{B_{uv}})} \tag{I.10}$$

where β_{1j} and β_{21} are obtained using fractional decomposition. These quantities are the same as in Theorem 2 satisfying (12). From the MGF $M_{\gamma_{uv}}^{UAV}(s)$ of γ_{uv}, we can obtain the PDF using the inverse Laplace transform as

$$P_{\gamma_{uv}}^{UAV}(x) = \sum_{j=1}^{m}\left(\beta_{1j}\mathcal{L}^{-1}\left[\frac{1}{(s - \frac{m}{A_{uv}})^j}\right]\right) + \beta_{21}\mathcal{L}^{-1}\left[\frac{1}{(s - \frac{1}{B_{uv}})}\right]$$

$$= \sum_{j=1}^{m}\left(\beta_{1j}x^{j-1}\exp(-\frac{mx}{A_{uv}})\frac{(-1)^j}{(j-1)!}\right) - \beta_{21}\exp(-\frac{x}{B_{uv}}). \tag{I.11}$$

In the same manner, the MGF of I is computed as

$$M_I(s) = \prod_{t=1}^{N} M_{\gamma_{tv}}(s) = \prod_{t=1}^{N}(1 - sB_{tv})^{-1}\left(1 - \frac{sA_{tv}}{m}\right)^{-m}$$

$$= \sum_{t=1}^{N} \frac{\alpha_t'}{s - \frac{1}{B_{tv}}} + \sum_{t=1}^{N}\sum_{j=1}^{m} \frac{\alpha_{t,j}}{(s - \frac{m}{A_{tv}})^j} \tag{I.12}$$

where α_t' and $\alpha_{t,j}$ are obtained using fractional decomposition. These quantities are the same as in Theorem 2 satisfying (13). The PDF of I can be computed as follows

$$P_I(x) = \mathcal{L}^{-1}[M_I(s)] = \mathcal{L}^{-1}\left[\sum_{t=1}^{N} \frac{\alpha_t'}{s - \frac{1}{B_{tv}}} + \sum_{t=1}^{N}\sum_{j=1}^{m} \frac{\alpha_{t,j}}{(s - \frac{m}{A_{tv}})^j}\right]$$

$$= \sum_{t=1}^{N} -\alpha_t'\exp\left(-\frac{x}{B_{tv}}\right) + \sum_{t=1}^{N}\sum_{j=1}^{m} \alpha_{t,j}\frac{(-1)^j x^{j-1}}{(j-1)!}\exp\left(-\frac{mx}{A_{tv}}\right). \tag{I.13}$$

Using the fundamental theorem of transformation of random variables, $P_{I'}$ is obtained as

$$P_{I'}(y) = \sum_{t=1}^{N} \alpha_t'(-1)\exp\left(-\frac{y-1}{B_{tv}}\right)$$

$$+ \sum_{t=1}^{N}\sum_{j=1}^{m} \alpha_{t,j}\frac{(-1)^j}{(j-1)!}\exp\left(-\frac{m(y-1)}{A_{tv}}\right)(y-1)^{j-1}. \tag{I.14}$$

In addition, the CDF of γ_{uv} is computed as

$$F_{\gamma_{uv}}^{UAV}(x) = \int_0^x P_{\gamma_{uv}}^{UAV}(y)dy = \sum_{j=1}^{m}\left(\beta_{1j}\frac{(-1)^j}{(j-1)!}\right.$$

$$\left.\left(\frac{m}{A_{uv}}\right)^{-j}\left(\Gamma(j) - \Gamma\left(j, \frac{mx}{A_{uv}}\right)\right)\right) - \beta_{21}B_{uv}\left(1 - \exp\left(-\frac{x}{B_{uv}}\right)\right). \tag{I.15}$$

The outage probability can be determined as

$$P_{out}(\gamma_{th}) = \int_1^\infty F_{\gamma_{uv}}(\gamma_{th}y)P_{I'}(y)dy = \sum_{j=1}^{m}\left[\beta_{1j}\frac{(-1)^j}{(j-1)!}\left(\frac{m}{A_{uv}}\right)^{-j}\left[\Gamma(j)\right.\right.$$

$$\left.\left.-\int_1^\infty \Gamma\left(j, \frac{m\gamma_{th}y}{A_{uv}}\right)P_{I'}(y)dy\right]\right] - \beta_{21}B_{uv}\left[1 - \int_1^\infty \exp(-\frac{\gamma_{th}y}{B_{uv}})P_{I'}(y)dy\right] \tag{I.16}$$

$$= \sum_{j=1}^{m}\left[\beta_{1j}\frac{(-1)^j}{(j-1)!}\left(\frac{m}{A_{uv}}\right)^{-j}\left[\Gamma(j) + \sum_{t=1}^{N}\alpha_t'\left(\sum_{p=1}^{n} B_{tv}\lambda_p\right.\right.\right.$$

$$\left.\Gamma\left(j, \frac{m\gamma_{th}(\theta_p B_{tv} + 1)}{A_{uv}}\right)\right) - \sum_{t=1}^{N}\sum_{j'=1}^{m}\alpha_{t,j'}\frac{(-1)^{j'}}{(j'-1)!}\left(\sum_{p=1}^{n}(A_{tv}/m)^{j'}\right.$$

$$\left.\left.\left.\lambda_p\theta_p^{j'-1}\Gamma\left(j, \frac{m\gamma_{th}(\theta_p(A_{tv}/m)+1)}{A_{uv}}\right)\right)\right]\right] - \beta_{21}B_{uv}\left[1 + \sum_{t=1}^{N}\alpha_t'\right.$$

$$\frac{\exp(-\frac{\gamma_{th}}{B_{uv}})}{\frac{\gamma_{th}}{B_{uv}} + \frac{1}{B_{tv}}} - \sum_{t=1}^{N}\sum_{j=1}^{m}\alpha_{t,j}\frac{(-1)^j}{(j-1)!}\left(\frac{\gamma_{th}}{B_{uv}} + \frac{m}{A_{tv}}\right)^{-j}\exp\left(-\frac{\gamma_{th}}{B_{uv}}\right)\Gamma(j)\right] \tag{I.17}$$

$$= \sum_{j=1}^{m}\left[\beta_{1j}\frac{(-1)^j}{(j-1)!}\left(\frac{m}{A_{uv}}\right)^{-j}\left(\Gamma(j) + \sum_{t=1}^{N}\alpha_t' f_{j,1}(B_{tv})\right.\right.$$

$$\left.\left.-\sum_{t=1}^{N}\sum_{j'=1}^{m}\alpha_{t,j'}\frac{(-1)^{j'}}{(j'-1)!}f_{j,j'}(A_{tv}/m)\right)\right] - \beta_{21}B_{uv}\left[1 + \exp\left(-\frac{\gamma_{th}}{B_{uv}}\right)\right.$$

$$\left.\left(\sum_{t=1}^{N}\frac{\alpha_t'}{\frac{\gamma_{th}}{B_{uv}} + \frac{1}{B_{tv}}} - \sum_{t=1}^{N}\sum_{j=1}^{m}\frac{\alpha_{t,j}}{\left(\frac{\gamma_{th}}{B_{uv}} + \frac{m}{A_{tv}}\right)^j}\frac{(-1)^j}{(j-1)!}\Gamma(j)\right)\right]. \tag{I.18}$$

The integrals in (I.16) involve the Gamma function with the exponential function. We use the Laguerre polynomial, defined as $\int_0^\infty e^{-x}f(x)dx = \sum_{p=1}^{n}\lambda_p f(\theta_p)$, to perform a numerical evaluation, where λ_p and θ_p are the weight and the zero factors of the n-th order Laguerre polynomials, respectively. The result in (I.17) is obtained using a change of variable. The expression of $f_{j,j'}(S)$ is provided in equation (14). Note that the result in (I.18) is the same as the outage probability expression presented in Theorem 2, which concludes the proof. $\blacksquare$